On new two-dimensional UHF radar observations of equatorial spread *F* at the Jicamarca Radio Observatory

F. S. Rodrigues[1], M. A. Milla[2], D. Scipion[3], J. M. Apaza[3], K. M. Kuyeng[3], J. Sousasantos[1], A. A. Massoud[1], and C. Padin[4]

[1]The University of Texas at Dallas, Richardson, USA
[2]Pontifical Catholic University of Peru, Lima, Peru
[3]Radio Observatorio de Jicamarca, Instituto Geofísico del Perú, Lima, Perú
[4]Ana G. Mendez University, Puerto Rico

Corresponding author: Fabiano S. Rodrigues (fabiano@utdallas.edu)

Abstract: We describe a mode for two-dimensional UHF (445 MHz) radar observations of *F*-region irregularities using the 14-panel version of the Advanced Modular Incoherent Scatter Radar (AMISR-14). We also present and discuss examples of observations made by this mode. AMISR-14 is installed at the Jicamarca Radio Observatory (JRO, 11.95° S, 76.87° W, ~0.5° dip latitude) in Peru and, therefore, allows studies of ionospheric irregularities at the magnetic equator. The new mode takes advantage of the electronic beam-steering capability of the system to scan the equatorial F-region in the east-west direction. Therefore, it produces two-dimensional views of the spatial distribution of sub-meter field-aligned density irregularities in the magnetic equatorial plane. The scans have a temporal resolution of 20 seconds and allow observations over a zonal distance of approximately 400 km at main F-region heights. While the system has a lower angular and range resolution than interferometric in-beam VHF radar imaging observations available at Jicamarca, it allows a wider field-of-view than that allowed with the VHF system. Here, we describe the mode, and present and discuss examples of observations made with the system. We also discuss implications of these observations for studies of ESF at the JRO.

Key Points:

- A new mode for two dimensional observations of F-region irregularities in the magnetic equatorial plane using AMISR-14 is described.
- Examples of observations are presented and illustrate the ability of the system to capture the genesis, evolution, and decay of sub-meter ESF irregularities.
- The benefits of the new mode are highlighted and implications of the new observations for studies and better understanding of ESF are discussed.

1 Introduction

Equatorial Spread-F (ESF) is the name given, for historical reasons, to signatures of irregularities in the ionospheric electron density observed by a variety of instruments, including ground-based radar systems, ionospheric scintillation monitors, airglow imagers, vertical radio sounders, *in-situ* satellite and rocket sensors and others (e.g., Woodman and LaHoz, 1976; McClure et al., 1977; Abdu et al., 1981; Rino et al., 1981; Tinsley, 1982; Kintner et al., 2007).

It is well recognized that ESF is produced by the so-called Generalized Rayleigh-Taylor plasma instability which finds favorable growth conditions in the nighttime magnetic equatorial ionosphere (Sultan, 1996). More recently, however, the collisional shear instability has also been suggested to play a role in ESF occurrence and morphology (Hysell and Kudeki, 2004; Kudeki et al., 2007). A substantial portion of what we have learned about ESF comes from ground-based radar observations. Woodman and La Hoz (1976), for instance, proposed an interchange mechanism process for the generation of ionospheric irregularities causing ESF based on radar measurements made at the magnetic equatorial site of the Jicamarca Radio Observatory.

While the first radar observations provided important information about the distribution of ESF irregularities as a function of height and local time, it was then realized that additional information about ESF morphology in the magnetic zonal direction was needed for a better understanding of the processes leading to ESF development. That realization, for instance, motivated the use of other systems such as the ARPA Long-Range Tracking and Instrumentation Radar (ALTAIR) for ionospheric studies (Tsunoda et al., 1979). ALTAIR is capable of steering, mechanically, its antenna and performing two-dimensional (2D) incoherent as well as coherent radar measurements of the ionosphere at low magnetic latitudes. The use of ALTAR for ionospheric studies, however, has been limited since the system is mainly used for other applications.

Subsequent investigations led to the development and application of interferometric radar imaging techniques for 2D ionospheric radio studies (Farley et al, 1981; Kudeki and Sürücü, 1991; Hysell, 1996; Woodman, 1997; Chau and Woodman, 2001; Rodrigues et al., 2017). These techniques have allowed the study of ESF irregularities in the magnetic equatorial plane with better spatial (and temporal) resolution than previously possible with other types of ground-based instruments. The field-of-view of the imaging technique, however, is constrained by the volume illuminated by the radar. In general, coherent backscatter radar imaging studies have been limited to angles of a few degrees off-zenith (e.g., Hysell and Chau, 2006; Rodrigues et al., 2008; Harding and Milla, 2013) and, therefore, covering zonal distances of only a few 10s of km at main F-region heights.

Developments towards using antenna arrays and electronic beam steering have also been made, and systems are now in place for ionospheric studies. The Middle and Upper Atmosphere (MU) radar in Japan (Fukao et al., 1988), the Equatorial Atmosphere Radar (EAR) in Indonesia (Fukao et al., 2003) and the Gadanki Mesophere-Stratosphere-Troposphere (MST) radar in India (Rao et al., 1995) are examples of systems capable of steering their beams electronically and make observations of field-aligned ionospheric irregularities. While these systems were intended, mainly, for studies of lower atmospheric regions (MST), their use for ionospheric observations

have been demonstrated, and they have provided significant contributions to our understanding of ionospheric turbulence at low and middle latitudes (e.g., Yamamoto et al., 1991; Fukao et al., 1991; Rishbeth and Fukao, 1995; Ajith et al., 2015; Dao et al., 2016; Joshi et al., 2019). These radar results have also contributed to motivating the development and deployment of new systems (e.g., Otsuka et al., 2009; Li et al., 2012, Patra et al., 2014) more focused on ionospheric studies.

In the American sector, efforts towards using phase array radar systems for ionospheric and space weather science led to the development of the Advanced Modular Incoherent Scatter Radar (AMISR) system. AMISR is a large, Ultra-High Frequency (UHF), high power (> 2MW) system designed to be capable of incoherent scatter measurements of the ionosphere. The system was also designed for remote operations and to be relocated from time to time. The first system was successfully deployed in Poker Flat, AK in 2007 and it is referred to as PFISR (Valentic et al., 2013). Two other systems were then deployed in Resolute Bay, Canada. The first Resolute Bay ISR (RISR-N) points to north and started operations in 2009. The second Resolute Bay ISR (RISR-C) points to the south and started observations in 2015 (Gilies et al., 2016). These two systems provide unique observations of the high latitude ionosphere.

In 2014, a smaller, low-power (~200 kW) version of AMISR referred to as AMISR-14 was deployed at the Jicamarca Radio Observatory for tests before planned deployment in Argentina. Given the reduced peak power and aperture when compared to a full AMISR system, initial tests carried out in 2014 focused on experiments related to coherent backscatter radar measurements of field-aligned irregularities (Rodrigues et al., 2015). The initial tests served to show that the electronic beam-steering capability can be used to investigate the spatial distribution of irregularities causing F-region echoes. At that time, however, only five beams pointed perpendicular to the geomagnetic field and in the zonal direction were used. Measurements were also made during a few days when only weak (mostly bottomside) ESF events occurred.

Unfortunately, after the tests, only a few new observations with different beam configurations could be made and operations had to stop due to several technical issues with the system. In 2019 we started repairs of the radar and since mid 2021 we have been running new experiments with AMISR-14. Here, we describe results of an experiment aimed at better understanding the spatio-temporal behavior of ESF events. More specifically, we present and discuss results related to a new mode that has been used for observations of the temporal evolution of the two-dimensional (2D) distribution of sub-meter ESF irregularities at the magnetic equatorial plane.

This report is organized as follows: Section 2 provides a summary of technical information about AMISR-14 and the new observation mode used in this study. In section 3 we present examples of ESF observations made by AMISR-14 and discuss the main results. In section 4 we summarize our results and highlight the potential of the observations for ESF studies at Jicamarca.

2 Instrumentation and Analyses

The Ultra-High Frequency (UHF) radar (AMISR-14) used for this study is derived from the Advanced Modular Incoherent Scatter Radar (AMISR), which can be described as a modular,

mobile radar system for radio remote sensing of the Earth's upper atmosphere and ionosphere and for studies of the space weather. AMISR was developed by SRI International under a grant from the National Science Foundation (NSF), and it is described in detail by Valentic et al. (2013). Here, we only summarize a few important technical points about AMISR that are relevant to our observations.

The most basic element of an AMISR system is the radar front-end Transmit/Receive (Tx/Rx) module, which is referred to as an Antenna Element Unit (AEU). The AEUs include a low-level RF circuity for phase control on transmit and receive, a 500-W solid state power amplifier (SSPA), a power supply, digital control and communication electronics, and a cross-dipole antenna. The arrangement of 32 AEUs onto an aluminum frame structure is referred to as a panel. Each panel has a control unit (PCU) containing a single board computer, which monitors in real-time various parameters for each AEU, including voltage, current, temperature, humidity and forward and reflected power levels.

A standard AMISR system contains 128 panels that are arranged, approximately, in a square configuration covering an area of about 30 x 30 m^2. Therefore, the standard AMISR system contains a total of 4096 AEUs that can operate in the 430 - 450 MHz frequency range and can produce a peak transmit power of about 2 MW. The antenna array can generate a beam with half-power width (HPBW) of 1.1^o. The antenna beam can be steered from pulse-to-pulse to over 10,000 preset directions within ±25^o-35^o boresight. Additionally, the SSPA can transmit pulses with lengths up to 2 ms with a 10% duty cycle. Finally, a variety of phase coding schemes can be applied to the pulse.

In 2010, a 14-panel version of AMISR (AMISR-14) was acquired from SRI International by Universidad Metropolitana, Puerto Rico (now Ana G. Méndez University - UAGM) through a grant from the NSF's Major Research Instrumentation (MRI) Program. The original plan for the system was for deployment in Argentina for geomagnetic conjugate studies with the Arecibo Observatory. Before moving to Argentina, however, the system was deployed near the magnetic equator at the Jicamarca Radio Observatory (11.95^o S, 76.87^o W, ~0.5^o dip latitude) in August 2014. The deployment at Jicamarca allowed tests of the system and collocated observations with other types of instruments for ionospheric research.

While the tests in 2014 could not confirm the ability of AMISR-14 to detect incoherent scatter echoes, they showed that the system is capable of detecting coherent scatter echoes produced by sub-meter field-aligned irregularities associated with ESF (Rodrigues et al., 2015; Hickey et al., 2015). More importantly, Rodrigues et al. (2015) showed that the system could provide two-dimensional views of ESF events. They proposed and carried out initial tests of a mode with 7 beam pointing directions for F-region observations. A total of 5 beams were pointed perpendicular to the geomagnetic field on the magnetic equatorial (East-West) plane. During these tests, bottomside ESF echoes were detected.

The 5-beam AMISR-14 observations in 2014 allowed a rough estimate of the spatial distribution of irregularities causing echoes and their evolution with time over a zonal distance of about 200 km at 300 km altitudes. While the angular and height resolution did not improve over interferometric techniques already in place at Jicamarca, AMISR-14 allows for observations over

a much wider zonal distance than currently possible. It allowed, for instance, Hickey et al. (2015) to investigate the correlation between large-scale ESF structures seen by airglow imagers and sub-meter irregularities seen b AMISR-14. Unfortunately, several technical issues interrupted the operations and only a few new observations were made with the system after the 2014 tests.

Repairs of the AMISR-14 system began towards the end of 2019 and were completed in mid 2021. Since then, new observations shave been made. Here, we present results of a new experiment for two-dimensional observations of ESF events. Similar to the 2014 experiment (Rodrigues et al., 2015), the 14 panels were arranged in a 7x2 array with the longest dimension aligned with the N/S direction. This produces half-power beam widths (HPBWs) of 2^o and 8^o in the N/S and E/W directions, respectively. As illustrated in Figure 1, a total of 10 pointing directions on the magnetic equatorial plane were used. The spacing in elevation between pointing directions was not even and was chosen to maximize perpendicularity (with respect to geomagnetic field) given the availability of pointing directions. Therefore, there is overlapping between some of the beam directions. The distribution, however, allows full coverage from 59.5^o of elevation to the west to 61.2^o to the east. Table 1 provides lists the specific azimuth and elevation angles for the beam directions. The observations were made at 445 MHz using an inter-pulse period (IPP) of 937.5 km, and a 28-bit coded pulse with 3 km bauds. A total of 16 pulses were transmitted in each beam direction. A summary of the main radar parameters for this mode is shown in Table 2.

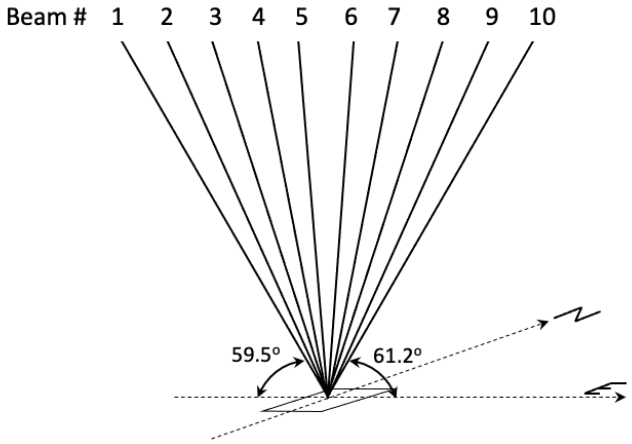

Figure 1. Diagram illustrating the antenna beam positions used in the AMISR-14 observations. Specific azimuth and elevation angles for all beam directions are provided in Table 1.

Table 1 – AMISR-14 pointing directions.

Beam Number	Azimuth (degrees)	Elevation (degrees)
1	-95.2	59.5
2	-96.5	65.8
3	-97.7	73.8
4	-99.50	78.3
5	-108.4	86.6
6	102.5	85.1
7	93.2	80.4
8	90.00	74.00
9	90.00	66.2
10	88.9	61.2

Table 2 – AMISR-14 experiment parameters.

Parameter	Value
Frequency	445 MHz
Bragg wavelength	0.34 m
Panel configuration	7 (N/S) x 2 (E/W)
Antenna HPBW (NS/EW)	1.4º (N/S) – 8.6º (E/W)
Nominal Peak power	185 kW
Number of beam positions	10
Pulses per beam position	16
Inter-Pulse Period (IPP)	937.5 km
Code length	28 bauds
Baud length	3.0 km
Sampling	1.5 km
Coherent integration	None
Incoherent integration	320 (2 seconds)

3 Results and Discussion

We now present and discuss examples of measurements using the 10-beam ESF radar mode. The measurements presented here were made on the night of July 16-17, 2021. We chose to report measurements made on this night because they capture different types of F-region irregularity events and illustrate well the benefits of the new 2D observations with respect to a better understanding of ESF. The geomagnetic Kp index did not exceed 3.0 any time on July 16 and 17, 2021. The observed (noontime) solar flux indices (F10.7) for these two days were 75 SFU and 77.4 SFU. Therefore, the observations can be described as having been made during geomagnetically quiet and low solar flux conditions.

Figure 2 shows the range-time-intensity (RTI) map for the observations made by the beam pointed closest to vertical (beam 5, see Table 1). For simplicity, from now on we refer to beam 5 as the vertical beam. The RTI map shows that the vertical beam only observed weak echoes most of the night, with only a weak plume detected in the pre-midnight sector, around 22:30 LT. The RTI map for the vertical beam also does not show echoes in the post-midnight sector. This is the scenario that a conventional radar system with a single beam would have observed.

Figure 3 now shows range-time-intensity (RTI) maps for the observations made in all the directions of the 10-beam F-region experiment. The RTI map for the westernmost pointing beam (beam 1) is on the top and the RTI map for the easternmost pointing beam (beam 10) is at the bottom. Figure 3 shows that RTI maps vary substantially from one beam to the next with some RTI maps showing strong echoes and well-developed plumes. The observations in Figure 3 illustrate the strong zonal variability in F-region irregularity activity within only a few 100s of km. We point out that the echoes observed around 03:12 LT in beams 6 to 10 are not caused by ionospheric F-region irregularities. They have been identified as clutter, that is, non-ESF echoes caused, for instance, by a satellite or meteor. We point out that the main echo comes from a narrow range but, in the RTI map, the sidelobes of the pulse code make the echo to appear coming from a range about 170 km long. This is because the pulse used in the experiment has 28

bauds with a 3-km baud (see Table 2) which gives an autocorrelation length of approximately 170 km. In addition to the narrow range, satellite and meteor echoes are often recognized in our RTI maps as having short duration, that is, lasting one or a few power profiles. The meteor echoes would come through low-elevation sidelobes and, as a result, would appear in the RTI maps at F-region heights.

The multi-direction observations made with the 10-beam F-region mode allow us to better understand the occurrence and dynamics of F-region irregularity structures over and around Jicamarca. For the presentation and discussions that follow, we focus on five distinct echoing layers or events that were identified in the RTI maps of Figure 3. These are indicated by black line parallelograms and are labelled S1-S5 in Figure 3.

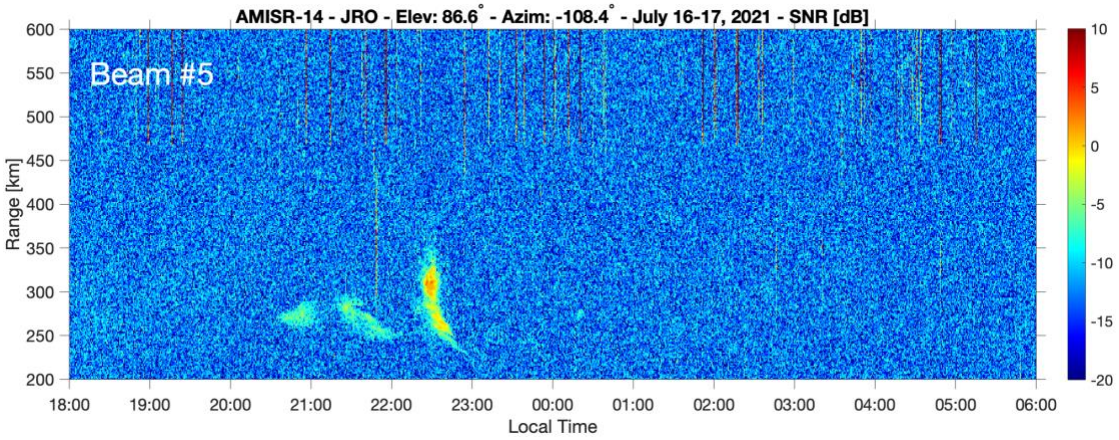

Figure 2 – Range-Time-Intensity (RTI) map for the observations made by beam pointed closest to zenith on July 16-17, 2021. The observations made by this beam only show weak F-region echoes with a poorly developed radar plume appearing around 22:30 LT. No post-midnight F-region echoes can be identified in the RTI map for the vertical beam.

3.1 Bottomside ESF structure (S1)

The top panel of Figure 4 shows again the RTI map for the observations made by the vertical beam (beam 5) of the F-region mode. The bottom panels show snapshots (or images) that allow visualization of the two-dimensional (zonal distance versus height) distribution of the echo-causing irregularities observed by the 10-beam mode.

While single "images" of the irregularity structures have a temporal resolution of 20 seconds, for this presentation we use averages of 5 consecutive images. This is done to reduce the effects of artifacts caused by clutter. The images presented here are similar to the so-called fan sector plots of the observations made by radars using electronic beam steering and presented in previous studies (e.g., Ajith et al., 2015). The specific times of the images are indicated in each panel. Additionally, a horizontal white line on the RTI map (top panel) indicates the time window where the images come from.

The RTI map of the vertical beam shows the occurrence of two weak bottomside echoing layers between about 20:30 LT and 22:10 LT. Bottomside layers can be described as RTI map

272 signatures of irregularities associated with ionospheric density perturbations created by the
273 ionospheric Rayleigh-Taylor instability. These perturbations, however, have less robust growth
274 than those associate with equatorial plasma bubbles and do not extend well into topside F-region
275 heights (e.g., Hysell et al., 2014a).

276 The images in the bottom panels of Figure 4 allow us to determine that the first bottomside layer
277 is generated right above Jicamarca. The images also allow us to determine that this echoing layer
278 not only has poor development in the vertical direction but is also limited to about ~100 km in
279 the zonal direction. First echoes appear around 20:36 LT, get stronger and, within minutes,
280 weaken and nearly disappear.
281

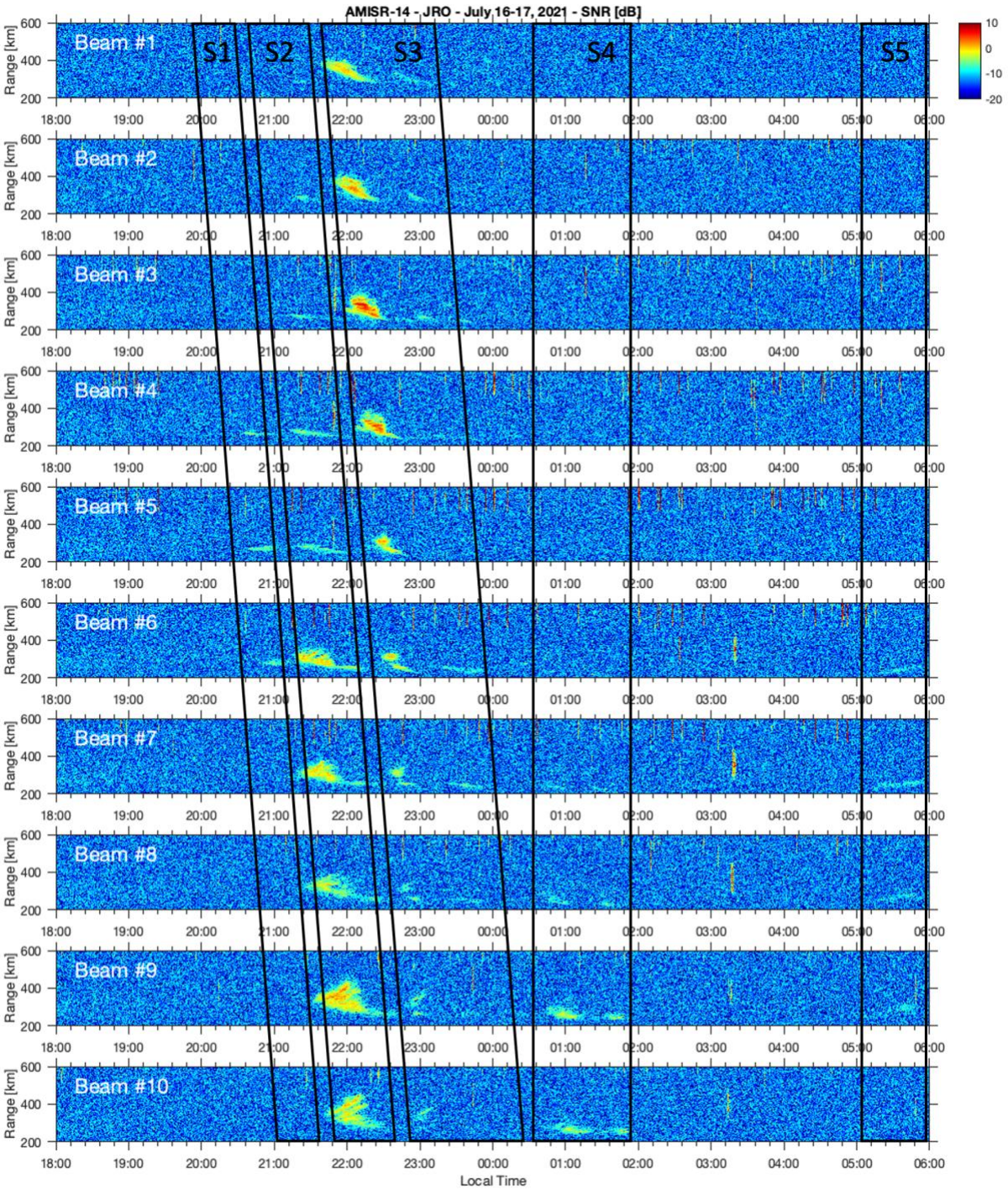

Figure 3 – Range-Time-Intensity (RTI) maps for the measurements made in all directions of the 10-beam F-region mode (see Table 1). Black line parallelograms labelled S1-S5 indicate five distinct echoing structures or events identified in the RTI maps and that are discussed one by one in this report.

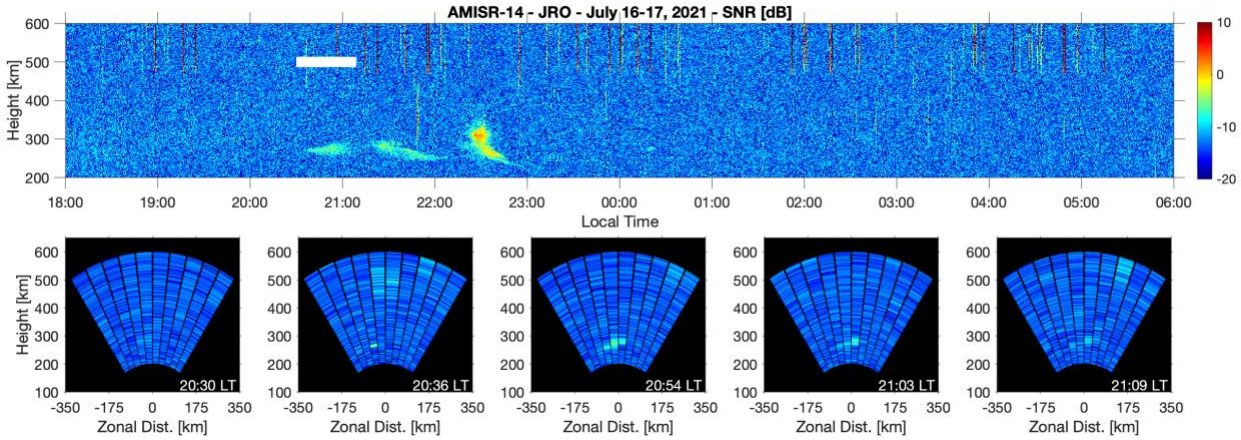

Figure 4 – The top panel shows the RTI map for the observations made by the beam closest to the zenith direction (beam 5). The bottom panels show 2D images of the spatial (height vs zonal distance) distribution of echo-causing sub-meter irregularities. These images are taken from the time window indicated by the horizontal white line in the RTI map. Specific times of the snapshots are also indicated in each panel.

3.2 Genesis of a radar plume (S2)

Figure 5 shows results for the second echoing structure (S2) identified in the 10-beam F-region mode RTI maps (Figure 3).

The sequence of images in Figure 5 are for a period between ~21:10 LT and 21:40 LT. The measurements are for a time when a second weak bottomside layer is seen in the RTI map for the vertical beam (top panel). The images, however, allow us to identify that a more severe ESF event developed eastward of Jicamarca, not being detected by the vertical beam.

The sequence of images shows that bottomside echoes above and around Jicamarca returned after 21:10 LT and that irregularities causing echoes developed vertically more than the irregularities associated with the first bottomside layer. The images also show that as the irregularities developed vertically, they also drifted zonally, and echoes were only captured by beams pointed to the east. This motion is in good agreement with the expectation of eastward plasma drifts in the equatorial F-region during evening hours (Fejer et al., 2005; Shidler et al., 2019) and with ionospheric irregularity drifts (e.g., Valladares et al., 2002; Muella et al., 2008). By 21:40 LT the images show a well-developed topside layer (radar plume) to the east of Jicamarca.

The images for this structure illustrate that the new mode can identify ESF events that would have been missed by a conventional single-beam radar system. In fact, the Jicamarca Unattended Long-term Investigations of the Ionosphere and Atmosphere – JULIA (Hysell and Burcham, 1998) system was operating on this day as well. JULIA is a single beam VHF (50 MHz) coherent scatter radar system that is dedicated to routine observations of ionospheric irregularities

including those associated with ESF (Zhan et al., 2018). JULIA also makes observations of irregularities in the magnetic equatorial plane but did not observe this structure as shown in Figure 6.

Differences in the RTI maps for AMISR-14 and JULIA are caused by a combination of different factors. For instance, JULIA observes Bragg scattering caused by 3-meter irregularities while AMISR-14 observes Bragg scattering from sub-meter (0.34 meter) irregularities. Additionally, differences in the observations are caused by differences in the aperture-power values of the two systems and in the direction of observations. JULIA radar uses an antenna with ~1° Half-Power Beam Width (HPBW) and is pointed near vertical with elevation (87°) and azimuth (-112.5°) angles closest to those of beam 5. In fact, despite the differences in irregularity scale sizes and radar parameters the JULIA RTI map (Figure 6) resembles the RTI map of beam 5 (Figure 2). Analyses of dual-frequency observations is outside the scope of this presentation and will be carried out in future studies.

Here we focus on highlighting the implication of the AMISR-14 observations for studies investigating the causal relationship between underlying background ionospheric conditions and ESF. For instance, studies have attempted to relate the magnitude of the pre-reversal enhancement (PRE) of the evening F-region vertical drifts and the development and severity of ESF as observed by conventional single-beam radars (Fejer et al., 1999; Smith et al., 2015; Smith et al., 2016). The 2D observations provided by AMISR-14 can allow one to determine, unequivocally, the occurrence and level of development of ESF so that it can be more accurately correlated with background plasma conditions measured at Jicamarca.

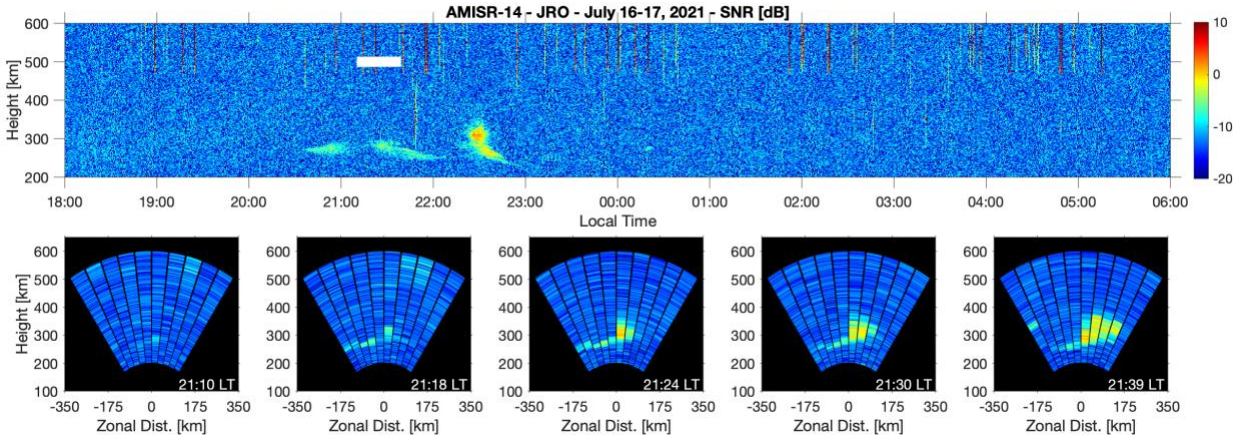

Figure 5 – Same as Figure 4. But now the images are for times when a radar plume was generated above Jicamarca and developed vertically while drifting to the east. Therefore, the images show the spatio-temporal evolution of a radar plume during its development. The RTI map for the vertical beam, however, continued to show only weak bottomside F-region echoes.

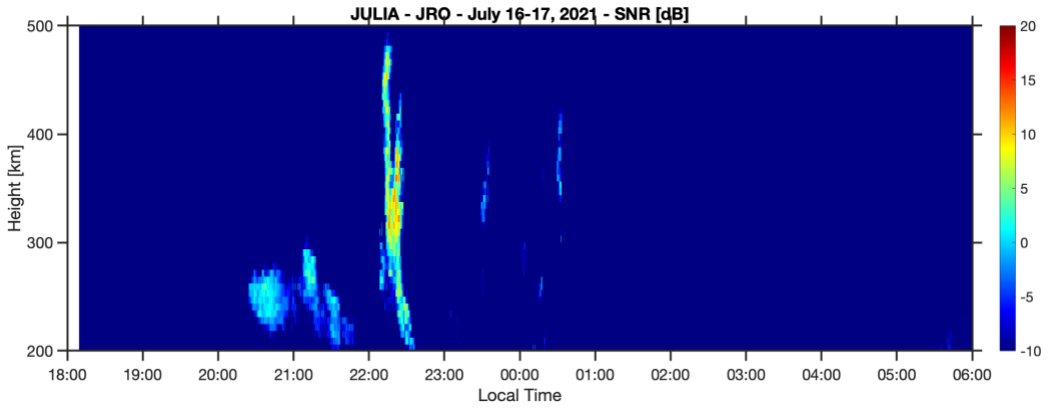

Figure 6 – RTI map for F-region measurements made by the VHF JULIA radar on July 16-17, 2021.

3.3 Decay of a radar plume (S3)

Figure 7 shows results for the third irregularity structure (S3) identified in the 10-beam F-region mode RTI maps (Figure 3).

The images show observations made when a small radar plume is seen in the RTI map for the vertical beam (top panel). The images are for a period between 21:40 LT and 22:50 LT indicated by the horizontal solid white line in the RTI map.

The images allow us to identify that the radar plume developed to the west of Jicamarca and outside of the field-of-view of AMISR-14. The plume then drifted eastward and entered the field-of-view of the westernmost beam at around 21:42 LT. The RTI maps and the images show that the plume was more vertically developed and that the echoes were stronger to the west of Jicamarca. The images also show that the echoes weaken and the plume decays as it moves to the east. The easternmost beam only detects faint F-region echoes.

The images for event S3 illustrate the ability of the AMISR-14 mode to identify, unambiguously, an ESF structure that developed non-locally, that is, a few 100s of km away from Jicamarca and that drifted into the field-of-view. It also illustrates the ability of the system to track the 2D dynamics of a decaying ESF event.

This example also has implications for studies investigating the underlying conditions leading to ESF development. For instance, Hysell et al. (2014b) used observations of the thermospheric and ionospheric state above Jicamarca to drive a numerical model of ESF. They found that the model could not predict the development of late ESF plumes similar to the one captured by AMISR-14 and presented in Figure 5. Hysell et al. (2014b) pointed out that the late plumes could have been caused by nonlocal influences, that is, conditions favoring instability development to the west (or east) of Jicamarca. The AMISR-14 observations provide experimental evidence that, indeed, late plumes could have been observed to the west, drifted zonally, and observed above Jicamarca at a later time during a decaying stage.

The wide field-of-view of the AMISR-14 images also allow identification between the spacing of plumes. The images in Figure 7 indicate that spacing between plumes was 300-350 km in the zonal direction. This is in good agreement with estimates of the spacing between equatorial plasma bubbles (EPBs) derived from airglow images by Makela et al. (2010). The average F10.7 index for July 16-17, 2021 was 76.2 SFU. For similar average solar flux conditions (77.5 SFU), Makela et al. (2010) found that EPBs had an average spacing of 339 km. We point out that the spacing between plumes can provide insight on the scale length of the initial density perturbations in the bottomside F-region triggering ESF as suggested by Makela et al. (2010).

Finally, we pointed out that the wide field of view of the system and its location near the magnetic equator provide unique observations that could be used to assist with the interpretation of the dynamics of ESF predicted by numerical models (Kherani et al., 2005; Huba et al., 2008; Retterer et al., 2010; Aveiro and Hysell, 2010; Yokoyama et al., 2014; Sousasantos et al., 2017).

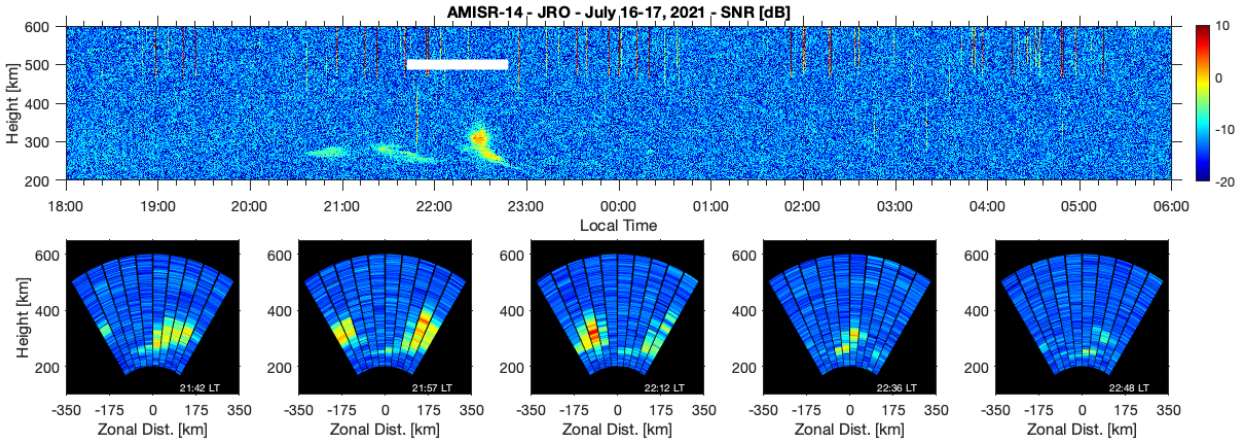

Figure 7 – Same as Figure 4. But now the images reveal the appearance of a second radar plume to the west of Jicamarca. The first image (leftmost) in the lower panels shows the first radar plume described in Figure 5 located to the east of Jicamarca, and the first echoes of the second radar plume to the west. As the two plumes drift eastward, the second plume enters the field-of-view of AMISR-14 and the echoes can be seen weaking and losing altitude. Therefore, the images show the spatio-temporal evolution of a decaying topside structure. The RTI map of the vertical beam shows the signatures of small radar plume.

3.4 Post-midnight ESF (S4)

Figure 8 shows results for the fourth irregularity structure (S4) identified in the 10-beam F-region mode RTI maps (Figure 3).

The images show observations made when no echoes are seen in the RTI map for the vertical beam (top panel). The images are for a period between approximately 00:48 LT and 02:26 LT indicated by the horizontal solid white line in the RTI map.

The images allow us to identify that while echoes are not seen above Jicamarca, they are present in the beams pointed to the east. The images show the occurrence of a post-midnight echoing structure that seems to appear to the east of Jicamarca at around 00:48 LT, but that did not

develop vertically and remained below 300 km altitude. The echoes also indicate only a very slow eastward motion. By 02:06 LT the echoes completely disappeared.

This example of measurements and images illustrate again that the AMISR-14 mode can capture events that would have been missed by a conventional, single-beam radar system. The observations also confirm the occurrence of post-midnight events during June solstice, low solar flux conditions even during geomagnetically quiet conditions as reported by Zhan et al. (2018) using JULIA observations. Additionally, the wide field-of-view of AMISR-14 observations suggest that the occurrence rate of post-midnight events around Jicamarca might be even higher than the rates reported by Zhan et al. (2018) using single beam JULIA measurements.

The observations also show that irregularities causing post-midnight echoes were generated locally, that is, within the field of view of AMISR-14. It has been suggested (Sekar et al., 2007) that post-midnight radar echoes could have been associated with "fossil" equatorial plasma bubbles, that is, bubbles that were produced far away from Jicamarca and drifted into the field of view after midnight. The AMISR-14 images indicate, however, that the irregularities causing echoes were generated locally. This agrees with recent VHF radar studies at Jicamarca that suggested that post-midnight echoes during June solstice would have been created locally. Zhan et al. (2018) found that the post-midnight ESF events would follow apparent F-region uplifts which indicate conditions favoring the growth of ionospheric Rayleigh-Taylor instability (e.g., Nicolls et al., 2006). Other studies also associated the occurrence of post-midnight ESF events to upward F-region vertical drifts (e.g., Yizengaw et al., 2013).

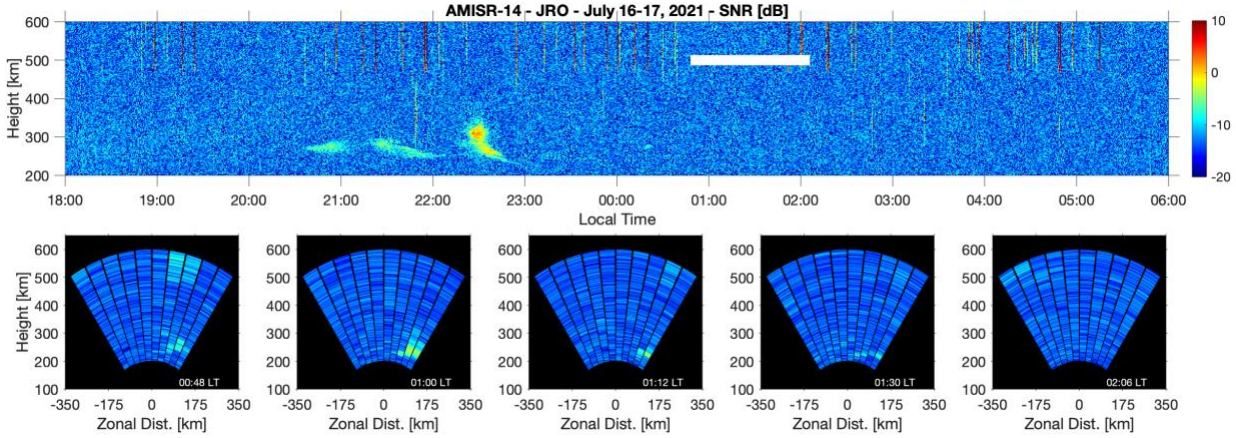

Figure 8 – Same as Figure 4. But now the images reveal the appearance of post-midnight F-region echoes to the east of Jicamarca that were missed by the vertical beam.

3.5 Pre-dawn ESF (S5)

Finally, Figure 9 shows results for the fifth irregularity structure (S5) identified in the 10-beam F-region mode RTI maps (Figure 3).

Again, the images show observations made when no echoes are seen in the RTI map for the vertical beam (top panel). The images are for a period between approximately 05:24 LT and 06:00 LT. The occurrence of these echoes follows a period where echoes were not detected by any of the AMISR-14 beams.

In this example, the images allow us to identify again that while echoes are not seen above Jicamarca. They originated, however, within the region covered by the beams pointed to the east. The images show the interesting development and occurrence of pre-sunrise F-region echoes. The echoes start at around 05:24 LT and are confined to a very narrow (~10 km in altitude) echoing layer. The image for measurements at 05:34 LT show that the layer can extend for at least about 150 km in the zonal direction and resemble a bottom-type layer. By 06:00 LT, no echoes can be identified in the images. Calculations of solar elevation show that dawn (-6^o solar elevation) occurred around 06:07 LT at E-region heights at Jicamarca and that at 06:00 LT, solar elevation was about -7.5^o. The observations show that around that time, solar ionization and current paths were enough to short-out polarization electric fields and suppress the pre-sunrise irregularities. Finally, the near-vertical JULIA observations in Figure 6 do not show the occurrence of pre-dawn echoes on this day. The climatological results of Zhan et al. (2018), however, do show that JULIA has detected echoes during pre-dawn hours in the past. Additionally, the JULIA detections also occurred during June solstice and geomagnetically quiet conditions. Future studies will investigate the underlying conditions leading to these pre-dawn events.

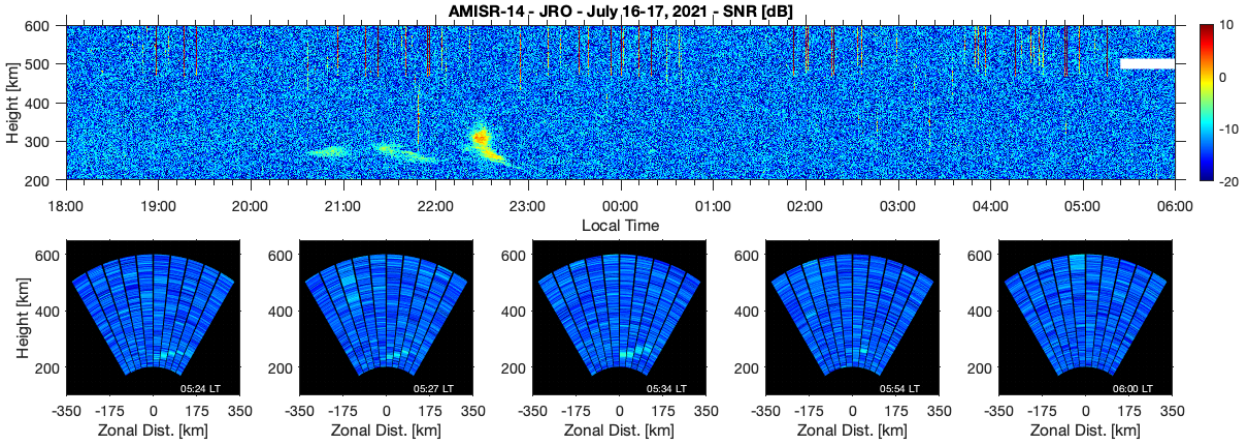

Figure 9 – Same as Figure 4. But now the images reveal the appearance of pre-dawn F-region echoes to the east of Jicamarca. Like in the case of the post-midnight event shown in Figure 8, the pre-dawn echoes and associated irregularities were missed by the vertical beam.

4 Concluding Remarks

AMISR-14 is a 14-panel version of the Advanced Modular Incoherent Scatter Radar (AMISR-14) that was installed at the Jicamarca Radio Observatory (JRO) in Peru in 2014. Several technical issues limited operations to a few E- and F-region observations with the system after deployment. It was possible, nevertheless, to show that the electronic steering capability of the system could contribute to studies of equatorial F-region irregularities though 2D coherent

backscatter radar measurements. For instance, observations made in 2014 used 5 beam directions in the magnetic equatorial plane and showed the detection of echoes associated with ESF (Rodrigues et al., 2015; Hickey et al., 2015).

As a collaboration between UT Dallas, JRO, and UAGM, AMISR-14 repairs started near the end of 2019 and were completed in mid 2021. Between July 2021 and February 2023, observations of the nighttime F-region have been made with AMISR-14. During daytime, experiments for different types of E- and F-region observations were run. Results of these observations will be presented in the future as studies are completed as part of student projects. Here, we focused on describing observations and results of a new mode used for nighttime 2D studies of the F-region.

The new mode uses 10 pointing directions and produces 2D views of the spatial distribution of sub-meter field-aligned ionospheric irregularities in the magnetic equatorial plane. The scans have a temporal resolution as short as 20 seconds and allow observations over a zonal distance of approximately 400 km at main F-region heights. While the system has a lower angular and range resolution than interferometric in-beam VHF radar imaging observations available at Jicamarca, it allows for a wider field-of-view than possible with the interferometric technique.

In this report we presented and discussed examples of observations made by this new 2D F-region mode on the night of July 16-17, 2022. We chose to report measurements made on this night because different types of ESF events were observed and because they illustrate well the potential of the new mode for a better understanding of ESF. The examples also illustrate the spatio-temporal dynamics of bottomside layers, topside plumes, post-midnight irregularities and pre-dawn irregularities. Below we summarize some of the experimental highlights and observational findings that are described in more detail in section 3:

- We showed that the new AMISR-14 2D F-region mode complements the single-beam F-region observations that have been made by VHF radars at Jicamarca. While the new mode does not have the spatial resolution of the images produced by interferometric in-beam imaging (Hysell and Chau, 2006), it allows observations of ESF events over a larger zonal distance (~400 km).

- We showed that the new AMISR-14 2D mode can contribute to the detection of ESF events that would have been missed by single-beam radar measurements. For instance, we showed the AMISR-14 detection of a radar plume that was missed by the collocated VHF JULIA radar. We also showed that AMISR-14 images allowed us to identify that while F-region echoes did start to develop over Jicamarca, it only became a full topside plume was only observed to the east of the site as it drifted zonally while developing. We pointed out that these observations will benefit, for instance, studies relating ESF to ionospheric-thermospheric conditions measured locally at Jicamarca (e.g., Smith et al., 2015).

- We showed that the new AMISR-14 mode can contribute to the identification of non-local ESF structures, that is, ESF structures that developed away from Jicamarca and that passed above the site in the late evening while decaying. We explained that the new observation mode can assist the interpretation of data-driven modeling efforts at Jicamarca (e.g., Hysell et al., 2014b). These efforts seek, for instance, a better understanding of late evening ESF

events that were observed above Jicamarca with JULIA but were not predicted by the model using local observations.

- We showed that the wide field of view of the AMISR-14 can contribute to observations of the spacing between radar plumes which, in turn, can provide insight on the initial bottomside F-region perturbations (seed waves) that trigger ESF (e.g., Makela et al., 2010). The example shown is in good agreement with independent observations made by airglow imagers under similar solar flux conditions.

- We showed that the new AMISR-14 2D F-region mode can contribute to the detection of post-midnight ESF events that would have been missed by a single-beam radar. We also showed that the AMISR-14 can provide information about the origin of post-midnight echoes. For instance, the AMISR-14 images for July 16-17, 2021, show that the irregularities causing echoes were generated locally, that is, within a few 10s of km of the radar site as suggested in recent studies (e.g., Zhan et al., 2018). The observations also indicate that the occurrence rate of post-midnight ESF layers near Jicamarca can be higher than previously reported by Zhan et al. (2018) based on single beam JULIA measurements.

- Finally, we also present an example of a pre-dawn echoing layer detected by the new AMISR-14 F-region mode and that occurred to the east of Jicamarca. Collocated vertical JULIA observations did not show the occurrence of these echoes over Jicamarca. AMISR-14 observations show that the pre-dawn echoes were limited in altitude and extended for only ~100km in the zonal direction.

We conclude by mentioning that Woodman (2009) inquired if the ESF problem had already been solved and that Hysell et al. (2014a) pointed out that, for many applications, the ESF problem could only be considered solved when it can be forecast. Hysell et al. (2014a) emphasized that models capable of reproducing morphologically accurate representations of ionospheric ESF structures would be an important milestone towards complete understanding of ESF. The F-region AMISR-14 mode presented here contributes with unique 2D observations of the morphology of ESF structures at the magnetic equator.

Declarations

Availability of data and materials

AMISR-14 data used in this study are available in this Box.com link:
https://zenodo.org/record/8225392

The geomagnetic Kp information was provided by the GFZ German Research Centre for Geosciences (https://kp.gfz-potsdam.de/en/).

The observed solar flux index (F10.7) information was provided by National Research Council Canada in partnership with the Natural Resources Canada (https://www.spaceweather.gc.ca/).

Competing interests

The authors declare that they have no competing interests.

Funding

This work was supported by NSF award AGS-1916055.

Authors' contributions

FSR proposed the study, analyzed the data, interpreted the results and wrote the manuscript. MAM contributed with the design of the AMISR-14 mode and interpretation of measurements. DS, JMA and KMK contributed with tasks related to repairs, operations and maintenance of AMISR-14. JS and AAM contributed with editing of the manuscript and interpretation of the measurements. CP contributed with the instrumentation (AMISR-14) used in this study.

Acknowledgements

We thank the technical staff of the Jicamarca Radio Observatory for their diligent work on AMISR-14 repairs and on operating the system for new observations. We also thank SRI international for their addressing numerous technical questions during the repair process.

611 **References**
612
613 Abdu, M. A., I. S. Batista, and J. A. Bittencourt (1981), Some characteristics of spread F at the
614 magnetic equatorial station Fortaleza, J. Geophys. Res., 86(A8), 6836–6842,
615 doi:10.1029/JA086iA08p06836.
616
617 Ajith, K. K., Ram, S. T., Yamamoto, M., Yokoyama, T., Gowtam, V. S., Otsuka, Y., Tsugawa,
618 T. and Niranjan, K. (2015), Explicit characteristics of evolutionary-type plasma bubbles
619 observed from Equatorial Atmosphere Radar during the low to moderate solar activity years
620 2010–2012. J. Geophys. Res. Space Physics, 120: 1371– 1382. doi: 10.1002/2014JA020878.
621
622 Aveiro, HC, Hysell DL (2010) Three-dimensional numerical simulation of equatorial F region
623 plasma irregularities with bottomside shear flow. J Geophys Res 115:11321.
624 doi:10.1029/2010JA015602.
625
626 Chau, J. L., and R. F. Woodman (2001), Three-dimensional coherent radar imaging at Jicamarca:
627 Comparison of different inversion techniques, J. Atmos. Sol. Terr. Phys., 63(2-3), 253–261,
628 doi:10.1016/S1364-6826(00)00142-5.
629
630 Dao, T., Otsuka, Y., Shiokawa, K., Tulasi Ram, S., and Yamamoto, M. (2016), Altitude
631 development of postmidnight F region field-aligned irregularities observed using Equatorial
632 Atmosphere Radar in Indonesia, Geophys. Res. Lett., 43, 1015– 1022,
633 doi:10.1002/2015GL067432.
634
635 Farley, D. T., H. M. Ierkic, and B. G. Fejer (1981), Radar interferometry: A new technique for
636 studying plasma turbulence in the ionosphere, J. Geophys. Res., 86(A3), 1467–1472,
637 doi:10.1029/JA086iA03p01467.
638
639 Fejer, B. G., Scherliess, L., and de Paula, E. R. (1999), Effects of the vertical plasma drift
640 velocity on the generation and evolution of equatorial spread F, J. Geophys. Res., 104(A9),
641 19859– 19869, doi:10.1029/1999JA900271.
642
643 Fejer, B. G., de Souza, J., Santos, A. S., and Costa Pereira, A. E. (2005), Climatology of F region
644 zonal plasma drifts over Jicamarca, J. Geophys. Res., 110, A12310, doi:10.1029/2005JA011324.
645
646 Fukao, S., J. P. McClure, A. Ito, T. Sato, I. Kimura, T. Tsuda, and S. Kato (1988), First VHF
647 radar observation of midlatitude F-region field-aligned irregularities, Geophys. Res. Lett., 8,
648 768–771.
649
650 Fukao, S., Kelley, M. C., Shirakawa, T., Takami, T., Yamamoto, M., Tsuda, T., and Kato, S.
651 (1991), Turbulent upwelling of the mid-latitude ionosphere: 1. Observational results by the MU
652 radar, J. Geophys. Res., 96(A3), 3725– 3746, doi:10.1029/90JA02253.
653
654 Fukao, S., H. Hashiguchi, M. Yamamoto, T. Tsuda, T. Nakamura, M. K. Yamamoto, T. Sato, M.
655 Hagio, and Y. Yabugaki (2003), Equatorial Atmosphere Radar (EAR): System description and
656 first results, Radio Sci., 38, 1053, doi:10.1029/2002RS002767.

Gillies, R. G., et al., First observations from the RISR-C incoherent scatter radar, Radio Sci., 51, 1645– 1659, doi:10.1002/2016RS006062, 2016.

Harding, B. J., and Milla, M. (2013), Radar imaging with compressed sensing, Radio Sci., 48, 582– 588, doi:10.1002/rds.20063.

Hickey, D. A., C. R. Martinis, F. S. Rodrigues, R. H. Varney, M. A. Milla, M. J. Nicolls, A. Strømme, and J. F. Arratia, Concurrent observations at the magnetic equator of small-scale irregularities and large-scale depletions associated with equatorial spread F, J. Geophys. Res. Space Physics, 120, doi:10.1002/2015JA021991, 2015.

Hysell, D. L. (1996), Radar imaging of equatorial F region irregularities with maximum entropy interferometry, Radio Sci., 31(6), 1567–1578, doi:10.1029/96RS02334.

Hysell, D. L., & Burcham, J. D. (1998). JULIA radar studies of equatorial spread F. Journal of Geophysical Research, 103(A12), 29,155–29,167. https://doi.org/10.1029/98JA02655

Hysell, D. L., and Kudeki, E. (2004), Collisional shear instability in the equatorial F region ionosphere, J. Geophys. Res., 109, A11301, doi:10.1029/2004JA010636.

Hysell, D. L., and Chau, J. L. (2006), Optimal aperture synthesis radar imaging, Radio Sci., 41, RS2003, doi:10.1029/2005RS003383.

Hysell, D. L., R. Jafari, M. A. Milla, and J. W. Meriwether (2014a), Data-driven numerical simulations of equatorial spread F in the Peruvian sector, J. Geophys. Res. Space Physics, 119, 3815–3827, doi:10.1002/2014JA019889.

Hysell, D. L., M. A. Milla, L. Condori, and J. W. Meriwether (2014b), Data-driven numerical simulations of equatorial spread F in the Peruvian sector: 2. Autumnal equinox, J. Geophys. Res. Space Physics, 119, 6981–6993, doi:10.1002/2014JA020345.

Huba, J. D., G. Joyce, and J. Krall (2008), Three-dimensional equatorial spread F modeling, Geophys. Res. Lett., 35, L10102, doi:10.1029/2008GL033509.

Joshi, L.M. , L.-C. Tsai, S.-Y. Su, Y. Otsuka, T. Yokoyama, M. Yamamoto, S. Sarkhel, K. Hozumi, C.-H. Lu (2019), Investigation of Spatiotemporal Morphology of Plasma Bubbles Based on EAR Observations, Journal of Geophysical Research: Space Physics, 10.1029/2019JA026839, 124, 12,10549-10563.

Kherani, A.E., Mascarenhas, M., De Paula, E.R. et al. A Three-Dimensional Simulation of Collisional-Interchange-Instability in the Equatorial-Low-Latitude Ionosphere. Space Sci Rev 121, 253–269 (2005). https://doi.org/10.1007/s11214-006-6158-x

Kintner, P. M., B. M. Ledvina, and E. R. de Paula (2007), GPS and ionospheric scintillations, Space Weather, 5, S09003, doi:10.1029/2006SW000260.

Kudeki, E., and F. Sürücü (1991), Radar interferometric imaging of field-aligned plasma irregularities in the equatorial electrojet, Geophys. Res. Lett., 18(1), 41–44, doi:10.1029/90GL02603.

Kudeki, E., Akgiray, A., Milla, M., Chau, J. L., and Hysell, D. L. (2007), Equatorial spread-F initiation: post-sunset vortex, thermo- spheric winds, gravity waves, J. Atmos. Solar-Terr. Phys., 69, 2416–2427.

Li, G., Ning, B., Abdu, M. A., Wan, W., and Hu, L. (2012), Precursor signatures and evolution of post-sunset equatorial spread-F observed over Sanya, J. Geophys. Res., 117, A08321, doi:10.1029/2012JA017820.

Makela, J. J., Vadas, S. L., Muryanto, R., Duly, T., and Crowley, G. (2010), Periodic spacing between consecutive equatorial plasma bubbles, Geophys. Res. Lett., 37, L14103, doi:10.1029/2010GL043968.

McClure, J. P., W. B. Hanson, and J. H. Hoffman (1977), Plasma bubbles and irregularities in the equatorial ionosphere, J. Geophys. Res., 82(19), 2650–2656, doi:10.1029/JA082i019p02650.

Muella, M.T.A.H. , E.R. de Paula, I.J. Kantor, I.S. Batista, J.H.A. Sobral, M.A. Abdu, P.M. Kintner, K.M. Groves, P.F. Smorigo (2008), GPS L-band scintillations and ionospheric irregularity zonal drifts inferred at equatorial and low-latitude regions, Journal of Atmospheric and Solar-Terrestrial Physics, Volume 70, Issue 10, Pages 1261-1272, ISSN 1364-6826, https://doi.org/10.1016/j.jastp.2008.03.013

Nicolls, M. J., Kelley, M. C., Vlasov, M. N., Sahai, Y., Chau, J. L., Hysell, D. L., Fagundes, P. R., Becker-Guedes, F., and Lima, W. L. C.: Observations and modeling of post-midnight uplifts near the magnetic equator, Ann. Geophys., 24, 1317–1331, https://doi.org/10.5194/angeo-24-1317-2006, 2006.

Otsuka, Y., Ogawa, T. & Effendy VHF radar observations of nighttime F-region field-aligned irregularities over Kototabang, Indonesia (2009), Earth Planet Sp 61, 431–437. https://doi.org/10.1186/BF03353159

Patra, A. K., P. Srinivasulu, P. P. Chaitanya, M. D. Rao, and A. Jayaraman (2014), First results on low-latitude E and F region irregularities obtained using the Gadanki Ionospheric Radar Interferometer, J. Geophys. Res. Space Physics, 119, 10,276–10,293, doi:10.1002/2014JA020604.

Rao, P. B., Jain, A. R., Kishore, P., Balamuralidhar, P., Damle, S. H. and Viswanathan, G. (1995), Indian MST radar. 1. System description and sample vector wind measurements in ST mode. Radio Sci., 30, 1125–1138.

Retterer, J. M. (2010), Forecasting low-latitude radio scintillation with 3-D ionospheric plume models: 1. Plume model, J. Geophys. Res., 115, A03306, doi:10.1029/2008JA013839.

Rino, C. L., R. T. Tsunoda, J. Petriceks, R. C. Livingston, M. C. Kelley, and K. D. Baker (1981), Simultaneous rocket-borne beacon and in situ measurements of equatorial spread F—Intermediate wavelength results, J. Geophys. Res., 86(A4), 2411–2420, doi:10.1029/JA086iA04p02411.

Rishbeth, H., and S. Fukao, A Review of MU Radar Observations of the Thermosphere and Ionosphere, Journal of geomagnetism and geoelectricity, 1995, Volume 47, Issue 7, Pages 621-637, https://doi.org/10.5636/jgg.47.621.

Rodrigues, F. S., Hysell, D. L., and de Paula, E. R.: Coherent backscatter radar imaging in Brazil: large-scale waves in the bottomside F-region at the onset of equatorial spread F, Ann. Geophys., 26, 3355–3364, https://doi.org/10.5194/angeo-26-3355-2008, 2008.

Rodrigues, F. S., M. J. Nicolls, M. A. Milla, J. M. Smith, R. H. Varney, A. Strømme, C. Martinis, and J. F. Arratia (2015), AMISR-14: Observations of equatorial spread F, Geophys. Res. Lett., 42, 5100–5108, doi:10.1002/2015GL064574.

Rodrigues, F. S., de Paula, E. R., and Zewdie, G. K.: High-resolution coherent backscatter interferometric radar images of equatorial spread F using Capon's method, Ann. Geophys., 35, 393-402, https://doi.org/10.5194/angeo-35-393-2017, 2017.

Sekar, R., Chakrabarty, D., Sarkhel, S., Patra, A. K., Devasia, C. V., and Kelley, M. C.: Identification of active fossil bubbles based on coordinated VHF radar and airglow measurements, Ann. Geophys., 25, 2099–2102, https://doi.org/10.5194/angeo-25-2099-2007, 2007.

Shidler, S. A., Rodrigues, F., Fejer, B. G., & Milla, M. (2019). Radar studies of height-dependent equatorial F region vertical and zonal plasma drifts. Journal of Geophysical Research: Space Physics, 124, 2058– 2071. https://doi.org/10.1029/2019JA026476

Smith, J. M., Rodrigues, F. S., and de Paula, E. R.: Radar and satellite investigations of equatorial evening vertical drifts and spread F, Ann. Geophys., 33, 1403–1412, https://doi.org/10.5194/angeo-33-1403-2015, 2015.

Smith, J. M., Rodrigues, F. S., Fejer, B. G., and Milla, M. A. (2016), Coherent and incoherent scatter radar study of the climatology and day-to-day variability of mean F region vertical drifts and equatorial spread F, J. Geophys. Res. Space Physics, 121, 1466– 1482, doi:10.1002/2015JA021934.

Sousasantos, J., Kherani, E. A., and Sobral, J. H. A. (2017), An alternative possibility to equatorial plasma bubble forecasting through mathematical modeling and Digisonde data, J. Geophys. Res. Space Physics, 122, 2079– 2088, doi:10.1002/2016JA023241.

Sultan, P. J. (1996), Linear theory and modeling of the Rayleigh-Taylor instability leading to the occurrence of equatorial spread F, J. Geophys. Res., 101(A12), 26875–26891, doi:10.1029/96JA00682.

Tinsley, B. A. : Field aligned airglow observations of transequatorial bubbles in the tropical F-region, J. Atmos. Terr. Phys., 44, 547– 557, doi:10.1016/0021-9169(82)90144-1, 1982.

Tsunoda, R. T., M. J. Baron, J. Owen, and D. M. Towle (1979), Altair: an incoherent scatter radar for equatorial spread F studies, Radio Sci., 14(6), 1111–1119, doi:10.1029/RS014i006p01111.

Valladares, C. E., Merriwether, J. W., Sheehan, R., and Biondi, M. A., Correlative study of neutral winds and scintillation drifts measured near the magnetic equator, J. Geophys. Res., 107(A7), doi:10.1029/2001JA000042, 2002.

Valentic T. et al. (2013), AMISR the advanced modular incoherent scatter radar, Proc. IEEE Int. Symp. Phased Array Syst. Technol., pp. 659-663.

Yamamoto, M., S. Fukao, R. F. Woodman, T. Ogawa, T. Tsuda, and S. Kato (1991), Mid-latitude E region field-aligned irregularities observed with the MU radar, J. Geophys. Res., 96, 15943-15949.

Yizengaw, E., Retterer, J., Pacheco, E. E., Roddy, P., Groves, K., Caton, R., and Baki, P. (2013), Postmidnight bubbles and scintillations in the quiet-time June solstice, Geophys. Res. Lett., 40, 5592– 5597, doi:10.1002/2013GL058307.

Yokoyama, T, Shinagawa H, Jin H (2014) Nonlinear growth, bifurcation, and pinching of equatorial plasma bubble simulated by three-dimensional high-resolution bubble model. J Geophys Res Space Phys 119:10474–10482. doi:10.1002/2014JA020708.

Zhan, W., Rodrigues, F., & Milla, M. (2018). On the genesis of postmidnight equatorial spread F: Results for the American/Peruvian sector. Geophysical Research Letters, 45, 7354–7361. https://doi.org/10.1029/2018GL078822.

Woodman, R. F., and C. La Hoz (1976), Radar observations of F region equatorial irregularities, J. Geophys. Res., 81(31), 5447–5466, doi:10.1029/JA081i031p05447.

Woodman, R. F. (1997), Coherent radar imaging: Signal processing and statistical properties, Radio Sci., 32(6), 2373–2391, doi:10.1029/97RS02017.

Woodman, R. F. (2009), Spread F – an old equatorial aeronomy problem finally resolved?, Ann. Geophys., 27, 1915–1934, https://doi.org/10.5194/angeo-27-1915-2009.